Astrophysical signatures of black holes in generalized Proca theories

Mostafizur Rahman* and Anjan A. Sen†
Centre for Theoretical Physics, Jamia Millia Islamia, New Delhi 110025, India

(Received 29 October 2018; published 31 January 2019)

Explaining the late-time acceleration is one of the most challenging tasks for theoretical physicists today. Infrared modification of Einstein's general theory of relativity (GR) is a possible route to model late-time acceleration. In this regard, vector-tensor theory, as a part of gravitational interactions on large cosmological scales, has been proposed recently. This involves generalization of a massive Proca Lagrangian in curved spacetime. Black hole solutions in such theories have also been constructed. In this paper, we study different astrophysical signatures of such black holes. We first study the strong lensing and time delay effect of such static spherically symmetric black hole solutions, in particular for the case of gravitational lensing of the star S2 by Sagittarius A* at the centre of Milky Way. We also construct the rotating black hole solution from this static spherically symmetric solution in Proca theories using the Newman-Janis algorithm and subsequently study lensing, time delay and black hole shadow effect in this rotating black hole spacetime. We discuss the possibility of detecting the Proca hair in future observations.

DOI: 10.1103/PhysRevD.99.024052

I. INTRODUCTION

Einstein's general theory of relativity (GR) is an extremely successful theory to describe gravity from solar system scales involving planetary motions up to cosmological scales describing the expansion of the Universe, formation of light elements, existence of cosmic microwave background radiation, formation of large scale structures. But the late-time acceleration of the Universe, first confirmed by SNIa observations two decades ago [1–5], is the first observed astrophysical phenomena, that attractive gravity fails to explain. Accelerated expansion in the Universe demands the existence of repulsive gravity at large cosmological scales. This can be done if one modifies either the matter part with exotic components having negative pressure or the gravity at large cosmological scales (see [6–9], for review on this topic). Although the cosmological constant (Λ), as introduced by Einstein to model a static Universe, is the simplest solution to the late-time acceleration of the Universe, the large discrepancy between the observed value of Λ and what we expect its value to be from the field theory point of view is the greatest obstacle to its successful explanation for the late-time acceleration of the Universe (also recent observations suggest tensions in ΛCDM with the data [10,11]). A consistent theory of quantum gravity is needed to solve this cosmological constant problem.

Going beyond Λ, whether to modify the matter sector or the gravity sector, scalar fields play the most important role in late-time acceleration of the Universe [6]. Scalar fields do exist in nature; Higgs field, which is the fundamental ingredient of standard model of particle physics [12], is the best example of a scalar field that exists in nature. Moreover, being a scalar, it can be naturally incorporated in a isotropic and homogeneous Universe. It also can give rise to repulsive gravity with its slow-roll property and hence can explain late-time acceleration. But these scalar fields have to be very light in order to slow-roll at large cosmological scales and without any mechanism to avoid their possible interactions with baryons, they give rise to long-range fifth force in baryons that is absent in solar system scales. To avoid such tensions, we need to have some screening mechanism that prevents the scalar field to interact with baryons on small scales, but allows the scalar field to give desired late-time accelerated expansion at large cosmological scales. The chameleon mechanism [13] and Vainshtein mechanism [14] are examples of such screening processes.

Among the scalar field models for infrared modification of gravity, the Galileon model is one of the most studied models [15–17]. It was first introduced as a natural extension of the DGP brane-world model [18] in the decoupling limit [19]. The Lagrangian for the Galileon field respects the shift symmetry and contains higher derivative terms. Despite this, the equation of motion for the Galileon field is second order and hence the theory is free from Ostragradsky ghosts [20]. One can also implement the Vainshtein mechanism in this model to preserve the local physics and to satisfy the solar system constraints. The general Galileon action with second-order equations of motion, contains nonminimal derivative coupling with Ricci and Einstein tensor. This is a subclass of more general

*mostafizur@ctp-jamia.res.in
†aasen@jmi.ac.in

Horndeski theories [21] which contain scalar-tensor interactions with second-order equations of motion on a curved background. Massive gravity theories [15,22] are other examples of general scalar-tensor theories giving second-order equations of motion.

Similar to scalar-tensor theories, one can also have consistent models of vector-tensor theory as a part of the gravitational interactions on large scales resulting the late-time acceleration in the Universe [23]. In Minkowski space, allowing the mass of the vector fields, leads to Proca Lagrangian. One can then generalize this massive Proca Lagrangian to curved spacetime. This has been done in a recent paper by Heisenberg [24], where a generalized massive Proca Lagrangian in curved background with second-order equations of motion has been proposed. This constitutes a Galileon-type self-interaction for the vector field including the nonminimal derivative coupling to gravity. Different cosmological aspects of such models as well as constraints from cosmological observations have been studied in several recent works [25]. In a recent paper, Heisenberg has studied, in a systematic way, different generalizations of Einstein gravity and their cosmological implications [26].

The recent results from Advanced Ligo experiment for measuring gravitational waves [27], have opened up the opportunity to probe astrophysical black holes. The latest gravitational wave measurements from two colliding neutron stars and its electromagnetic counterparts [28], have confirmed the validity of GR for these astrophysical processes. This put extremely tight constraints on different modified gravity theories based on scalar fields [29], explaining the late-time acceleration in the Universe. In a recent work, Jimenez and Heisenberg [30] have put forward vector models for dark energy based on a Proca Lagrangian with $c_{\rm gw} = 1$ making it consistent with latest Ligo observations for neutron star merger. But the model can still give nontrivial predictions for gravitational waves.

To probe any gravitational theory at astrophysical scales, black hole are the best candidates. Recently, Heisenberg *et al.* have constructed hairy black hole solutions in generalized Proca theories [31]. For power-law coupling, they found a class of asymptotically flat hairy black hole solutions. These are not exact solutions but are iterative series solutions up to $\mathcal{O}(1/r^3)$ which matches excellently with the numerical solutions. These are hairy black hole solution in a modified gravity scenario and it is extremely interesting to study their astrophysical signatures to probe the underlying modified gravity theory.

Gravitational lensing is one of most interesting astrophysical phenomena due to gravitational effects of massive bodies. It is broadly the bending of light due to the curvature of the spacetime and as the curvature of the spacetime depends on the gravitational properties of massive bodies, one can directly constrain different properties of a massive body like its mass or angular momentum, by observing its gravitational lensing effect. In solar system, through lensing effects, observers first confirmed the validity of Einstein GR. But in solar system, the effect is pretty weak with deflection angle much small compared to 2π [32–34]. But it can be large in the vicinity of strong gravitating objects like black holes, where the photon can circle in closed loops around the black hole many times due to the strong gravitational effect, before escaping. There exists a sphere around the black hole called a "photon sphere," where the deflection angle for the photon can even diverge. Gravitational lensing in the spacetime of Schwarzschild black holes was first studied by Virbhadra and Ellis [35] and later it was extended to Reissner-Nordstorm [36] and Kerr black holes [37], black holes in brane-world models [38] and Galileon models [39], in extra dimensions with the Kalb-Ramond field [40], and so on. As strong gravitational lensing in the vicinity of black holes probes different properties of the black holes, it is also useful to probe different modified gravity theories as standard Schwarzschild or Kerr black solutions get modified in different versions of modified gravity theories. Moreover, through gravitational lensing, one can probe the region around black holes, known as a "black hole shadow" [41]. The shape and size of the black hole shadow is a direct probe for the black hole spacetime and hence the underlining gravity theory. With the prospects of the Even Horizon telescope [42] as well as telescopes like SKA [43], one can resolve the black hole shadow with great accuracy and hence probing modified gravity through such observations is possible in near future. In this paper, we study the strong lensing phenomena for the black hole spacetimes in generalized Proca theories. Throughout the paper, we have used the geometrical unit $G = c = 1$.

II. HAIRY BLACK HOLE SOLUTION IN GENERALIZED PROCA THEORIES

The action for general Proca theory is given by [24,30,31,44]

$$S = \int d^4x\,\sqrt{-g}\left(F + \sum_{i=2}^{6}\mathcal{L}_i\right), \tag{1}$$

with

$$\begin{aligned}
\mathcal{L}_2 &= G_2(X), \qquad \mathcal{L}_3 = G_3(X)\mathcal{A}^{\mu}{}_{;\mu},\\
\mathcal{L}_4 &= G_4(X)R + G_{4,X}[(\mathcal{A}^{\mu}{}_{;\mu})^2 - \mathcal{A}_{\nu;\mu}\mathcal{A}^{\mu;\nu}] - 2g_4(X)F,\\
\mathcal{L}_5 &= G_5(X)G_{\mu\nu}\mathcal{A}^{\nu;\mu} - \frac{G_{5,X}}{6}[(\mathcal{A}^{\mu}{}_{;\mu})^3 - 3\mathcal{A}^{\mu}{}_{;\mu}\mathcal{A}_{\sigma;\rho}\mathcal{A}^{\rho;\sigma}\\
&\quad + 2\mathcal{A}_{\sigma;\rho}\mathcal{A}^{\rho;\nu}\mathcal{A}_{\nu}{}^{;\sigma}] - g_5(X)\tilde{F}^{\alpha\mu}\tilde{F}^{\beta}_{\mu}\mathcal{A}_{\beta;\alpha},\\
\mathcal{L}_6 &= G_6(X)L^{\mu\nu\alpha\beta}\mathcal{A}_{\nu;\mu}\mathcal{A}_{\beta;\alpha} + \frac{G_{6,X}}{2}\tilde{F}^{\alpha\beta}\tilde{F}^{\mu\nu}\mathcal{A}_{\mu;\alpha}\mathcal{A}_{\nu;\beta}.
\end{aligned} \tag{2}$$

Here $F = -F_{\mu\nu}F^{\mu\nu}/4$. The functions $G_2 - G_6$ as well as g_4 and g_5 depend on $X = -\mathcal{A}_\mu\mathcal{A}^\mu/2$. We denote $G_{i,X} = \partial G_i/\partial X$. The vector field $\mathcal{A}^\mu$ has nonminimal couplings with

spacetime curvature through $L^{\mu\nu\alpha\beta} = \mathcal{E}^{\mu\nu\rho\sigma}\mathcal{E}^{\alpha\beta\gamma\delta}R_{\rho\sigma\gamma\delta}/4$, where $\mathcal{E}^{\mu\nu\rho\sigma}$ is the Levi-Civita tensor and $R_{\rho\sigma\gamma\delta}$ is the Riemann tensor. The dual strength tensor $\tilde{F}^{\mu\nu} = \mathcal{E}^{\mu\nu\alpha\beta}F_{\alpha\beta}/2$. The Einstein-Hilbert term $M_{\rm pl}^2/2$ is contained in $G_4(X)$.

To describe the black holes in this general Proca theory, one assumes a static spherically symmetric spacetime:

$$ds^2 = -A(r)dt^2 + B(r)dr^2 + C(r)(d\vartheta^2 + \sin^2\vartheta d\varphi^2), \quad (3)$$

together with the vector field $\mathcal{A}_\mu = (\mathcal{A}_0(r), \mathcal{A}_1(r), 0, 0)$. Here $A(r)$, $B(r)$, $\mathcal{A}_0(r)$, and $\mathcal{A}_1(r)$ are arbitrary functions of r. In [31,44], the following action has been considered for general Proca theory:

$$S = \int d^4x\sqrt{-g}\left(\frac{M_{\rm Pl}^2}{2}R + \beta_3\mathcal{A}^\mu_{;\mu}X + F\right). \quad (4)$$

Up to $\mathcal{O}(1/r^3)$, the Black hole solution for such theory is given by [31,44]

$$\begin{aligned} A(r) &= 1 - \frac{2}{r} - \frac{P^2}{6r^3} + \mathcal{O}(1/r^4) \\ B(r)^{-1} &= 1 - \frac{2}{r} - \frac{P^2}{2r^2} - \frac{P^2}{2r^3} + \mathcal{O}(1/r^4) \\ C(r) &= r^2 \end{aligned} \quad (5)$$

where, we have set $r = r/M$, where M is the mass of the black hole. Throughout the paper, all the distances are measured in the unit of the mass of the black hole ($M = 1$) unless otherwise specified. Here P is Proca hair, related to the time component of the vector field as $\mathcal{A}_0 = (P - P/r - P/(2r^2))M_{\rm Pl} + \mathcal{O}(1/r^3)$. We set $P = P/M_{\rm Pl}$ where $M_{\rm Pl}$ is the Planck mass. Clearly, the metric satisfies asymptotically flat condition, $\lim_{r\to\infty}A(r) = \lim_{r\to\infty}B(r) = 1$. Note that, in the limit $P \to 0$, i.e., when the Proca hair P vanishes, the above metric elements reduce to that of Schwarzschild metric.

III. LENSING EFFECT IN STRONG FIELD LIMIT IN A STATIC, SPHERICALLY SYMMETRIC METRIC

Before considering the spacetime of our interest, we review the gravitational lensing effect in Strong Field Limit (SFL) in a general asymptotically flat, static and spherically symmetric spacetime. In this section we discuss about the main concepts and different observables related to gravitational lensing in the strong field limit following Ref. [45].

A. Observables in the strong field limit

Any generic static, spherically symmetric spacetime can be described by the line element (3). In order to study the photon trajectory, we will assume that the equation [35,45,46]

$$C'(r)A(r) - A'(r)C(r) = 0 \quad (6)$$

admits at least one positive solution and the largest positive solution of this equation is defined as the radius of photon sphere, r_m. We further assume that $A(r)$, $B(r)$ and $C(r)$ are finite and positive for $r \geq r_m$ [45]. Since the spacetime admits spherical symmetry, we can restrict our attention to equatorial plane ($\vartheta = \pi/2$) without losing any generality. Now we can formulate the lensing problem. Consider a black hole situated at the origin. A photon with impact parameter u incoming from a source situated at r_S, deviates while approaching it. Let the photon approach the black hole at a minimum distance r_0 and then deviate away from it. An observer situated at r_R detects the photon [see Fig. 1]. In the strong field limit, we consider only those photons whose closest approach distance r_0 is very near to r_m and hence the deflection angle α can be expanded around the photon sphere, r_m or equivalently minimum impact parameter u_m. When the closest approach distance r is greater than r_m, it just simply gets deflected (it may complete several loops around the black hole before reaching the observer). When it reaches a critical value $r_0 = r_m$ (or $u = u_m$), α diverges and the photon gets captured. Following the method developed by Bozza [45], one can show that this divergence is logarithmic in nature and the deflection angle can be written as

$$\alpha(\theta) = -\bar{a}\ln\left(\frac{\theta}{\theta_m} - 1\right) + \bar{b} \quad (7)$$

where subscript 'm' denotes function evaluated at $r = r_m$. θ is the incident angle to the observer whereas $\theta_m = u_m\sqrt{A(r_R)/C(r_R)}$ corresponds to the incoming photon with minimum impact factor, $u_m = \sqrt{C_m/A_m}$. When $\theta \leq \theta_m$, the photon gets captured. The parameters $\bar{a}$ and $\bar{b}$ are called the Strong Lensing coefficients whose functional forms are given in Eqs. (35)–(36) of Ref. [45].

With the help of Eq. (7), we can calculate the observables for strong lensing corresponding to any given static and spherically symmetric metric using the lens equation. The corresponding observables are (i) position of the innermost image, θ_m, (ii) the angular separation between the first relativistic image (outermost image) with the innermost image, s, and (iii) relative flux between different images, $\mathcal{R}$. In order to do so, we introduce co-ordinate independent lens equation: $\alpha = \theta - \theta_S + \phi_{RS}$, where θ and θ_S denote the angles that are measured at the receiver position and the source position, respectively, while ϕ_{RS} is the angle between the azimuthal coordinate of source and observer [47]. The quantity α is geometrically invariant which in asymptotically flat limit, coincides with the deflection angle. If $\bar{\theta}$ denotes the impact angle as seen from the source, then angle measured from source position becomes $\theta_S = \pi - \bar{\theta}$. Let γ be the angle between the optic axis (the line joining the observer and the lens) and the line joining

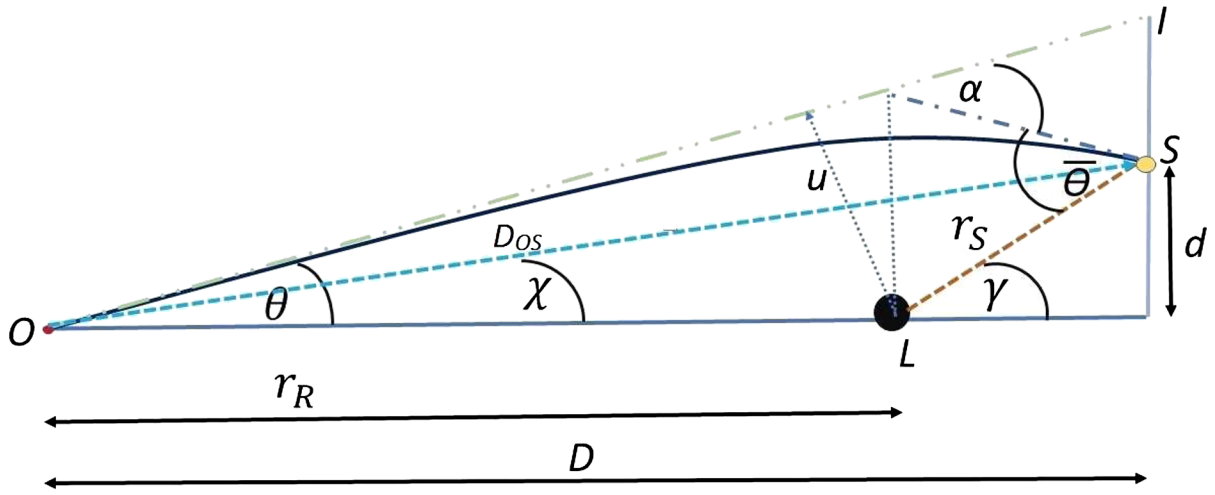

FIG. 1. A schematic diagram of the lensing system has been presented. Light from source S get lensed by the black hole L and incident on the observer O with an angle θ. Image is formed at I. The line joining O and L is called the Optic axis [40].

the lens and the source (see Fig. 1). Note that $\phi_{RS} = \pi - \gamma$. Then the lens equation connecting the observer and source position takes the form

$$\gamma = \theta + \bar{\theta} - \alpha(\theta) \tag{8}$$

This equation is known as the Ohanian lens equation [48] and as discussed in Ref. [49], is the best approximate lens equation in asymptotically flat spacetime. Since both the source and observer are situated far away from the black hole, $\bar{\theta}$ can be approximated as $\bar{\theta} = \theta r_R / r_S$. With this condition and using Eqs. (7) and (8), one can obtain the position of the nth-order image [45],

$$\theta_n = \theta_m \left(1 + \exp\left(\frac{\bar{b} + \gamma - 2n\pi}{\bar{a}}\right)\right), \tag{9}$$

where n corresponds to the number of windings around the black hole. When $n \to \infty$, θ_n becomes θ_m. So θ_m represents the position of innermost relativistic image. In simplest of situation, we consider that the outermost image (first relativistic image) θ_1 is resolved as a single image and all the other images packed together at θ_m [40,45]. Then the angular separation between these two images is defined as [45]

$$s = \theta_1 - \theta_m = \theta_m \exp\left(\frac{\bar{b} + \gamma - 2\pi}{\bar{a}}\right) \tag{10}$$

Magnification of the image is defined as the ratio of solid angle to the observer with a lens to the solid angle without lens, i.e., $\mu = \sin\theta d\theta / \sin\chi d\chi$, where χ is the angle between source to observer with respect to the optic axes (see Fig. 1). Note that lens equation Eq. (8) does not have any term that contains χ. So using the relation, $r_S \sin\gamma = D_{\rm OS} \sin\chi$ and considering $D_{\rm OS} \gg r_S$, one can easily show that the magnification of nth relativistic image can be written as [45]

$$\mu_n = \left(\frac{D_{\rm OS}}{r_S}\right)^2 \frac{\theta_m^2 e_n (1 + e_n)}{\bar{a} \sin\gamma}, \qquad e_n = \exp\left(\frac{\bar{b} + \gamma - 2n\pi}{\bar{a}}\right).$$

where $D_{\rm OS}$ is the distance between the source and observer. The ratio of magnification, hence the flux from the first relativistic image to all the other images, is given by [45]

$$\mathcal{R} = 2.5 \log_{10}\left(\frac{\mu_1}{\sum_{n=2}^{\infty} \mu_n}\right) = \frac{5\pi}{\bar{a} \ln 10} \tag{11}$$

If we have a precise knowledge of γ and observer to lens distance r_R, then we can predict strong lensing co-efficient $\bar{a}$, $\bar{b}$ and minimum impact parameter u_m by measuring $\mathcal{R}$, s, θ_m. Then by comparing them with the values predicted by given theoretical models, we can identify the nature of the black hole.

B. Time delay in strong field gravitational lensing

In this section we briefly review the Time Delay effect in a static, spherically symmetric spacetime following the method developed by Bozza and Manchini [50]. From the discussion in the previous section, it is clear that formation of multiple images is a key feature of strong lensing and generally the time taken by different photons following different paths (which correspond to different images) are not the same. So there are some time delay between different images. Moreover time delay between the images will depend on which side of the lens the images are formed. When both the images are on the same side of the lens, time delay between m and n th relativistic image can be expressed as [50]

$$\Delta T^{s}_{mn} = -u_m 2\pi(m-n) + 2\sqrt{u_m}\sqrt{\frac{B_m}{A_m}}\left(\exp\left(\frac{\bar{b}+\gamma-2m\pi}{2\bar{a}}\right) - \exp\left(\frac{\bar{b}+\gamma-2n\pi}{2\bar{a}}\right)\right) \tag{12}$$

The sign of γ depends on which side of the source images are formed. When the images are formed on the opposite side of the lens time delay between m and n th relativistic image can be expressed as [50]

$$\Delta T^{o}_{mn} = -u_m(2\pi(m-n)-2\gamma) + 2\sqrt{u_m}\sqrt{\frac{B_m}{A_m}}\left(\exp\left(\frac{\bar{b}+\gamma-2m\pi}{2\bar{a}}\right) - \exp\left(\frac{\bar{b}-\gamma-2n\pi}{2\bar{a}}\right)\right) \tag{13}$$

We need instruments with high observational precision in order to find the contribution from the second term. Thus for practical purposes, we can approximate the time delay by its first term's contribution. In terms of θ_m one can get an interesting result when both the images are formed in the same side of the lens. Then time delay between first and second relativistic image can be expressed as [51]

$$\Delta T^{s}_{12} = \theta_m 2\pi r_R \tag{14}$$

In principle, using this formula, we can get a very accurate estimate for the distance of the black hole. Note that for a distant observer, $A(r_R)$ practically becomes 1 and θ_m can be written as $\theta_m = r_m/\sqrt{A_m r_R^2}$. Using Eq. (14), we can find an interesting result given by

$$r_m^2 A(r_m) = \left(\frac{\Delta T^{s}_{12}}{2\pi}\right)^2. \tag{15}$$

This equation beautifully relates an observational parameter, the time delay ΔT^{s}_{12} between first and second relativistic image with a theoretical parameter, the metric function $A(r)$ evaluated at $r = r_m$. Thus, one can verify a given theoretical model by solving this equation using the observational data of ΔT^{s}_{12}.

IV. NUMERICAL ESTIMATION OF DIFFERENT OBSERVABLES FOR GRAVITATIONAL LENSING OF THE STAR S2 BY SGR A*

In this section we will numerically estimate the values of different observable parameters related to strong lensing for a spacetime described by Eqs. (3)–(5). For this purpose, we take the nature of the super massive black hole (SMBH) at the center of our Galaxy (Sgr A*) is given by solutions of second order generalized Proca theories. Here we take the star S2 as the source. This star revolves around the SMBH in a highly elliptic orbit with orbital time period around 15.92 years and has the minimum average distance from it. In the early 2018, it had been at its periapse position. Previous studies have shown that the magnification of images is maximum when the star reaches its pariapse position [51]. This gives us an unique opportunity to observe different lensing parameters in this time and thus make it possible to verify different theories of gravity. In this section, we first reconstruct the lensing system using the data given in Ref. [51,52] and then numerically calculate different observables related to strong lensing in this scenario.

A. The lensing system

The mass of black hole at the center of our Galaxy is estimated to be $4.01 * 10^6 M_\odot$ which is located at a distance 7.8 kpc away from us [53]. S2 is one of the star with the minimum average distance from it (S-102 has even smaller minimum average distance but it is 16 times fainter than S2 [54]). As stated earlier, it was at its periapse position in early 2018 where one expect to have maximum magnification [51]. So we have used it as a source for gravitational lensing. Moreover, S2 has radius of few solar radii, so one can treat it as point source. It's orbital motion (along with other short-period stars around SMBH) has been studied over 20 years mainly by two groups, one at Keck Observatory while the other with New Technology Telescope (NTT) and with Very Large Telescope (VTT) [52]. From those studies, we now have a precise understanding about its orbital motion. Its orbital parameters are reported in Table I [51,52]. Its position (r_S, γ), can be expressed in terms of the orbital parameters of the system [51,55],

$$r_S = \frac{\varrho(1-e^2)}{1+e\cos\xi} \tag{16}$$

TABLE I. Orbital parameters for S2. Its orbit can be described by an ellipse with ϱ as the semimajor axis and e as the eccentricity of the orbit. The inclination angle i denotes the angle between the ellipse and a reference plane in the line of sight. Ω and ω describes the position angle of the ascending node and the periapse anomaly with respect to the ascending node respectively. The orbital time period is described by T. T_0 describes the epoch when it reaches the periapse position [51,52].

Orbital Parameter	ϱ (pc)	T (yr)	e	T_o (yr)	i (deg)	Ω (deg)	ω (deg)
Value	4.54×10^{-3}	15.92	0.89	2018.37	45.7	45.9	244.7

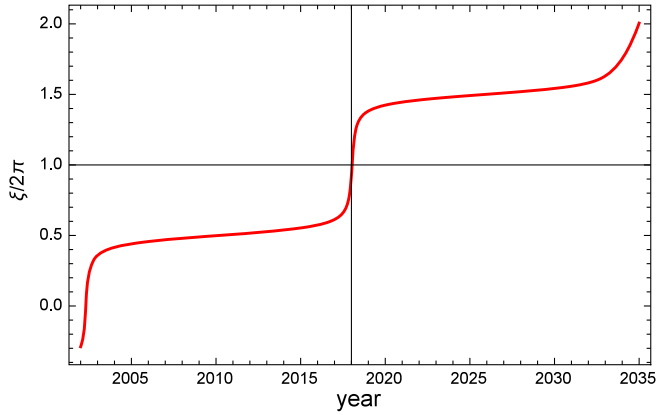

FIG. 2. Orbital position of S2 as a function of time have been presented. Here ξ represents the anamoly angle from the periapse position. Previous studies have shown that the maximum magnification of the images will be obtained when S2 is in its periapse position, i.e., when $\xi = 2\kappa\pi$, where κ is an integer [51]. The plot indicates that this had been achived in early 2018.

$$r_R \simeq D_{\rm os} = 7.8 \text{ kpc} \tag{17}$$

$$\gamma = \arccos[\sin(\xi + \omega)\sin i], \tag{18}$$

where $D_{\rm os}$ is the distance between observer and the source, ϱ is the major semiaxis, e is the eccentricity, i is the inclination of the normal of the orbit with respect to the line of sight, ω is the periapse anomaly with respect to the ascending node. ξ is the anomaly angle from the periapse, determined by the differential equation and initial condition

$$\frac{T}{2\pi}\frac{(1-e^2)^{3/2}}{(1+e\cos\xi)^2}\dot{\xi} = 1$$
$$\xi(T_0) = 2\kappa\pi \tag{19}$$

where T is the orbital time period of S2 and T_0 is the epoch of periapse and κ be any integer. We have plotted anomaly angle as a function of time in Fig. 2. From the plot, we can see that the star reached its periapse position in early 2018.

B. Numerical estimation of different lensing parameters

In this section, we present the numerical estimation of different observational parameters considering the SMBH at the center of our Galaxy as a lens and the star S2 as a source. Here we have considered that nature of black hole spacetime is given by solutions of second order generalized Proca theories presented in Eq. (5) and the S2 star is at its pariapse position. The radius of the photon sphere is given by the largest positive solution of the equation [see Eq. (6)]

$$12r^3 - 36r^2 - 5P^2 = 0 \tag{20}$$

Clearly, one can see that in the limit $P = 0$, the radius of the photon sphere is reduces to $r_m = 3$, representing photon circular orbit in Schwarzschild spacetime. By solving the above equation, one can express the radius of the photon sphere as

$$r_m = 1 + \frac{2}{\sqrt[3]{K1}} + \frac{\sqrt[3]{K1}}{2} \tag{21}$$

where,

$$K1 = \left[\left(\frac{5P^2}{3} + 8\right) + \frac{\sqrt{5}}{3}\sqrt{P^2(5P^2+48)}\right]$$

As stated earlier, we assumed that $A(r)$, $B(r)$, and $C(r)$ are finite and positive for $r \geq r_m$. But here $B(r)$ fails to remain positive for $P \geq 2.48$ at $r = r_m$ and hence in our analysis we will concentrate in the range $P < 2.48$. In Table II, we have presented the numerical estimation of different observational parameters namely the angular position of the innermost image θ_m, the angular separation between inner- and outermost image s, the relative magnification of the outermost relativistic image with the other images $\mathcal{R}$ and

TABLE II. Numerical estimations of the observables related to strong lensing (θ_m, s, $\mathcal{R}$, ΔT^s_{12}) have been presented. A comparison between the values of the observables obtained from generalized Proca theories (Proca BH) to those obtained from the Reissner-Nordström black hole (RN BH) have also been presented. Here the parameter "hair" corresponds to Proca hair P in the case of Proca BH and charged hair q in the case of RN black holes. Note that, hair $= 0$ case corresponds to the Schwarzschild black hole. Here the SMBH at the center of our Galaxy is taken as the lens whereas the star S2 is taken as the source. The observables have been calculated at the epoch of periapse of the star S2 (early 2018).

	θ_m in μas		s in μas		$\mathcal{R}$		ΔT^s_{12} in sec	
Hair	Proca BH	RN BH	Proca BH	RN BH	Proca BH	RN BH	Proca BH	RN BH
0	19.0033	19.0033	0.182 214	0.182 214	15.708	15.708	32.6484	32.6484
0.3	19.0191	18.713	0.185 641	0.188 735	15.5854	15.5434	32.6755	32.1498
0.6	19.066	17.7691	0.196 129	0.214 982	15.2132	14.934	32.7563	30.5281
0.9	19.143	15.7962	0.214 176	0.314 308	14.5764	13.0677	32.8885	27.1385

the time delay between first and second relativistic image ΔT^s_{12} (formed on the same side of the lens). We also compare the results with those obtained from Reissner-Nordström (RN) black hole solution with charge q whose line element can be expressed as [56,57]

$$ds^2 = -\left(1-\frac{2M}{r}+\frac{q^2}{r^2}\right)dt^2+\left(1-\frac{2M}{r}+\frac{q^2}{r^2}\right)^{-1}dr^2 + r^2(d\theta^2+\sin^2\theta d\phi^2) \tag{22}$$

In Table II, "hair" corresponds to Proca hair P in the case of generalized Proca black holes [Eq. (5)] and charged hair q in the case of Reissner-Nordström (RN) black holes [Eq. (22)]. We also have plotted the observables as a function of hair parameter for these two black hole spacetime in Fig. 3. From Table II, we found out that in the case of generalized Proca black holes, angular position of the innermost image θ_m increases as the hair parameter increases which is contrary to the RN case. This means that the size of the innermost Einstein ring is bigger for the generalized Proca black hole spacetime than those obtained from RN spacetime for the same value of the hair parameter. The angular separation s increases with the increase of the hair parameter similar to case of RN black hole spacetime while the relative flux $\mathcal{R}$ decreases with the increase of the hair parameter. From Table II, one can see that ΔT^s_{12} increases with the increase of hair parameter for the case of generalized Proca black holes which is contrary to the RN case. Note that the size of the innermost Einstein ring θ_m (or, the time delay between first and second relativistic image ΔT^s_{12}) is maximum for the case $q=0$ (Schwarzschild black hole) in static, spherically symmetric spacetime predicted by general relativity. So any value of θ_m (or ΔT^s_{12}) greater than those predicted in Schwarzschild spacetime implies the existence of Proca hair. Thus by measuring the size of the innermost Einstein ring (or the time delay between first and second relativistic image) in a static, spherically symmetric spacetime, one can observationally verify the "no-hair" theorem [58].

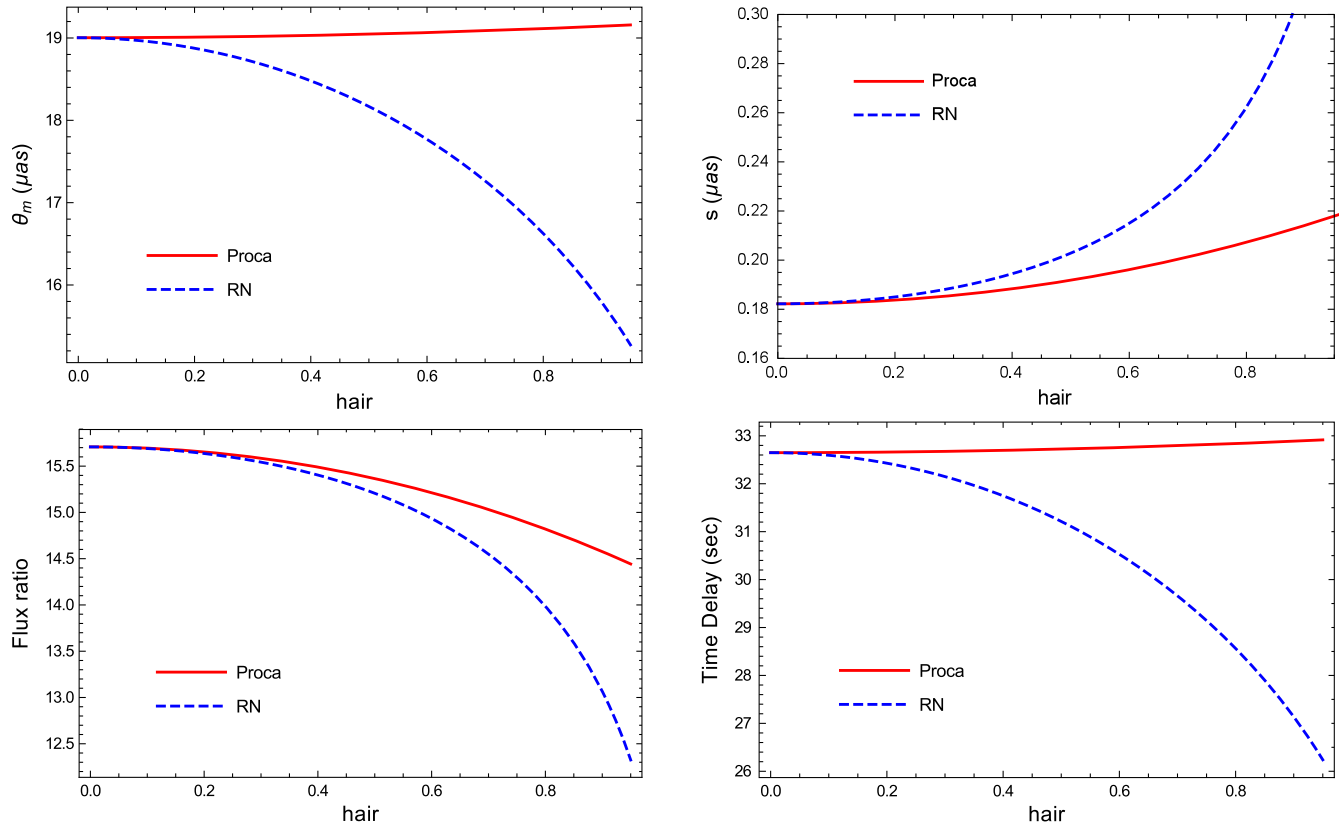

FIG. 3. Variation of different observables: (a) angular position of innermost image θ_m, (top-left corner) (b) the angular difference between the outermost and inner images s (top-right corner) (c) Flux ratio of the innermost image with respect to the others, $\mathcal{R}$ (bottom-left corner) and (d) Time delay between first and second relativistic image that formed on the same side of the lens ΔT^s_{12} (bottom-right corner) as a function of the hair parameters. Here the parameter "hair" corresponds to Proca hair P in the case of generalized Proca black holes and charge hair q in the case of Reissner-Nordström black holes. The solid red lines indicates the behavior of the observables as function Proca hair P for generalized Proca black holes whereas the blue dashed lines indices the variation of the observables as a function charge hair q for Reissner-Nordström black holes.

TABLE III. In Table II, numerical estimation of different observables related to strong lensing (θ_m, s, $\mathcal{R}$, ΔT^s_{12}) for metric (5) have been presented where we have considered metric components up to order $\mathcal{O}(1/r^3)$ only. This table shows the percentage modification of the observables when the contribution from the next leading order [$\mathcal{O}(1/r^4)$] is taken into account. As one can see for most of the cases, the deviation is below 1%.

	Percentage modification of the value when $\mathcal{O}(1/r^4)$ is included in the metric for the observables			
Proca hair	θ_m	s	$\mathcal{R}$	ΔT^s_{12}
0.3	0.055 051 6	0.444 458	0.111 209	0.055 051 6
0.6	0.214 403	1.702 92	0.447 742	0.214 403
0.9	0.4623	3.571 28	1.031 14	0.4623

Now, in order to probe the Proca hair, one have to observationally measure both the position of the innermost image θ_m and angular septation s. From Table II, we can see that the angular separation between the images is $\sim\mathcal{O}(10^{-1})$ μ arcsec, which is too hard to detect with present technologies.

Before doing further study with Proca black hole, we want to discuss an important issue regarding the validity of our estimates for different astrophysical parameters. As mentioned in Sec. II, the solution (5) for Proca black hole that we consider in our study, is not an exact solution of the Einstein equations, but an approximated analytical solution which agrees well with the full numerical solution up to order $\mathcal{O}(1/r^3)$. Although this is ok for regions away from the black hole horizon, but for near-horizon regions, analytical approximation may break down. To see how far it affects the numerical estimates of different observables, we consider solution up to order $\mathcal{O}(1/r^4)$ (next order) [44], calculate different observables and study the percentage deviations from the corresponding values for solution up to order $\mathcal{O}(1/r^3)$. The result is shown in Table III. As one can see, for most of the cases, the deviation is around 1% or less, except for the parameter s with high value of Proca hair, when the deviation is around 3%. Hence, as long as the errors in future observational estimates for these parameters are larger than these percentage deviations, our results are reliable.

V. LENSING OF ROTATING PROCA BLACK HOLES

In the previous section, we have studied the bending of light ray trajectory in the presence of a static and spherically symmetric black hole. But several observations indicate that the super massive black hole in the center of our Galaxy possesses angular momentum [59]. So for observational perspective, it is important to consider the lensing effect for a rotating black hole. Moreover, the spacetime geometry is much more richer in this case. So from pure theoretical point of view, we can expect some interesting result will emerge when we consider strong lensing effect around a rotating black hole. Indeed, previous studies has showed that the caustic points are no longer aligned with the optical axis for the rotating black hole, but shifted in according to the rotation of the black hole and now they have a finite extension [60]. In this present section, we will discuss the gravitational lensing effect for a more general rotating black hole. First we calculate the metric for a rotating black hole in generalized Proca theories using Newman-Janis algorithm and then study the null trajectories in this spacetime.

A. Null geodesic equation and photon trajectory

Applying Newman-Janis algorithm [61] to the metric.(5) and retaining only terms up to the order $\mathcal{O}(\frac{P^2}{r^3})$, we found out the stationary, axisymmetric solution to Einstein's field equation which in Boyer-Lindquist coordinates (t, r, ϑ, ϕ) [62] can be written as

$$\begin{aligned} ds^2 = &-\left[1-\frac{2r}{\rho^2}-\frac{P^2}{6\rho^2 r}\right]dt^2 - \frac{4a\sin^2\vartheta}{\rho^2}\left[r+\frac{P^2}{8}+\frac{P^2}{6r}\right]dtd\phi \\ &+\frac{\rho^2}{\Delta}dr^2+\rho^2 d\vartheta^2 \\ &+\left[r^2+a^2+\frac{2ra^2\sin^2\vartheta}{\rho^2}+\frac{P^2a^2\sin^2\vartheta}{2\rho^2}\left(1+\frac{1}{r}\right)\right] \\ &\times\sin^2\vartheta d\phi^2 \end{aligned} \tag{23}$$

where $a = L/M^2$, where L and M denotes the angular momentum and mass of the black hole, respectively. The Proca field in this case is turned out to be

$$\mathcal{A}_\mu = \left(\tilde{\mathcal{A}}_0, -\frac{\tilde{\mathcal{A}}_0\rho^2}{\Delta}\frac{1}{\sqrt{\tilde{A}\,\tilde{B}}} + \left(\tilde{\mathcal{A}}_0+\tilde{\mathcal{A}}_1\sqrt{\frac{\tilde{B}}{\tilde{A}}}\right)\left(1-\frac{a^2\sin^2\theta}{\Delta}\right), 0, \tilde{\mathcal{A}}_1\sqrt{\frac{\tilde{B}}{\tilde{A}}}a\sin^2\theta\right), \tag{24}$$

where "tilde" denotes the components after complexification. We have checked that Eqs. (23) and (24) together satisfy the Einstein's equation for an axisymmetric metric for a rotating Proca black hole up to order $\mathcal{O}(1/r^4)$. As our original nonrotating black hole solution is valid up to order $\mathcal{O}(1/r^3)$, we can safely take the metric given by Eq. (23) for a rotating Proca black hole for further study.

We can also identify the quantity a in Eq. (23) as the specific angular momentum of the black hole. The functions ρ and Δ is given by

$$\rho^2 = r^2 + a^2\cos^2\vartheta \tag{25}$$

$$\Delta = r^2 + a^2 - 2r - \frac{P^2}{2}\left(1+\frac{1}{r}\right) \tag{26}$$

Here, also, we have set $r = r/M$ and $P = P/M_{\rm Pl}$. In the limit of vanishing Proca hair, i.e., $P \to 0$, the solution coincides with the Kerr black hole. Horizon of the black hole is a surface where $\Delta = 0$ and outer horizon is determined by the largest possible solution of the equation, which in this case turns out to be

$$r_H = \frac{2}{3} - \frac{-16 + 12a^2 - 6P^2}{3\sqrt[3]{4}\sqrt[3]{4\sqrt{K} - 144a^2 + 180P^2 + 128}} + \frac{\sqrt[3]{4\sqrt{K} - 144a^2 + 180P^2 + 128}}{6\sqrt[3]{4}} \tag{27}$$

where the function $K = 2(6a^2 - 3P^2 - 8)^3 + (-36a^2 + 45P^2 + 32)^2$. It is easy to see in the limit a, $P \to 0$, and radius of the horizon turns out to be $r_H = 2$ as expected for the Schwarzschild case.

Null geodesic equations can be obtained by using the Hamilton-Jacobi equation [57]. For the metric (23), the relevant geodesic equations are given by

$$\rho^2\dot{r} = \sqrt{R(r)} \tag{28}$$

$$\rho^2\dot{\vartheta} = \sqrt{\Theta(\vartheta)} \tag{29}$$

$$\rho^2\dot{\phi} = \frac{a}{\Delta}(r^2 + a^2 - aJ) + \frac{P^2 a}{\Delta}\left(\frac{1}{2}+\frac{1}{3r}\right) + (J\sin^{-2}\vartheta - a), \tag{30}$$

where

$$R(r) = (r^2 + a^2 - aJ)^2 - P^2 a\left(\frac{1}{2}+\frac{1}{3r}\right) - \Delta(Q + (J-a)^2) \tag{31}$$

$$\Theta(\vartheta) = Q - (J^2\sin^{-2}\vartheta - a^2)\cos^2\vartheta. \tag{32}$$

In Eqs. (28)–(30), the dot indicates derivative with respect to some affine parameter λ. In Eqs. (31) and (32), Q denotes a constant of separation called Carter constant, J is the angular momentum of the photon with respect to the axis of the black hole. In our analysis, we have set $p_t = -E = -1$ by a suitable choice of affine parameter.

Since we are interested in studying the photon trajectory in an isolated black hole spacetime, we can ignore the effect of other celestial bodies on the photon trajectory and can approximate the spacetime at a large distance from the black hole as flat Minkowski spacetime. We will assume that both the source and observer are situated at a large distance from the black hole. Now we can formulate the lensing problem as follows: the initial photon trajectory starts off as a straight line. If there were no black hole, then it would continue to follow this straight line trajectory. But because of the presence of the black hole, its path gets deviated from this initial trajectory near the black hole. Finally, it approaches the observer along this deviated path. In this scenario, we can relate the constant of motion Q and J in terms of a set of geometric quantities (ψ_R, u, h) [63]. Here the inclination angle ψ_R denotes the angle between the initial photon trajectory and the equatorial plane. The projected impact parameter u describes the minimum distance of the projected photon trajectory on the equatorial plane from the origin if there were no black hole and, finally, the height of the light ray trajectory at u from the equatorial plane is denoted by h.

Let (α, β) denote the celestial coordinate of the image as seen by an observer sitting on (r_R, ϑ_R) in Boyer-Lindquist coordinate. The coordinate α and β represents the apparent perpendicular distance of the image from the axis of symmetry and its projection on the equatorial plane, respectively [57]. Taking into consideration that the observer is situated far away from the black hole and using Eqs. (28)–(32), we can express α and β as [57,64]

$$\alpha = -r_R^2 \sin\vartheta_R \left.\frac{d\phi}{dr}\right|_{r_R\to\infty} = \frac{J}{\sin\vartheta_R} \tag{33}$$

$$\beta = r_R^2 \left.\frac{d\vartheta}{dr}\right|_{r_R\to\infty} = h\sin\vartheta_R \tag{34}$$

Taking the asymptotic limit $\vartheta_R = \pi/2 - \psi_R$ and $\alpha = u$, we can finally express the constants of motion in terms of geometric parameters of the incoming ray as

$$J \approx u\cos\psi_R \tag{35}$$

$$Q \approx h^2\cos^2\psi_R + (u^2 - a^2)\sin^2\psi_R \tag{36}$$

VI. BLACK HOLE SHADOW ANALYSIS

In this section, we will describe the shadow of rotating black hole. For nonrotating black hole, it is just a black circular disc in the observable sky with a radius that corresponds to the position of the photon sphere. As we will see, things goes a bit interesting in the case of rotating black hole.

We will use the celestial coordinates (α, β) given in Eqs. (33)–(34) to give a description of the shadow. For simplicity, let us assume that the observer is sitting on the equatorial plane. Then using Eqs. (33)–(36), it is easy to check that photons reaching from an generic point $(\alpha/r_R, \beta/r_R)$ can be characteristic by $J = -\alpha$ and $Q = \beta^2$. In our calculation we have considered that positive angular

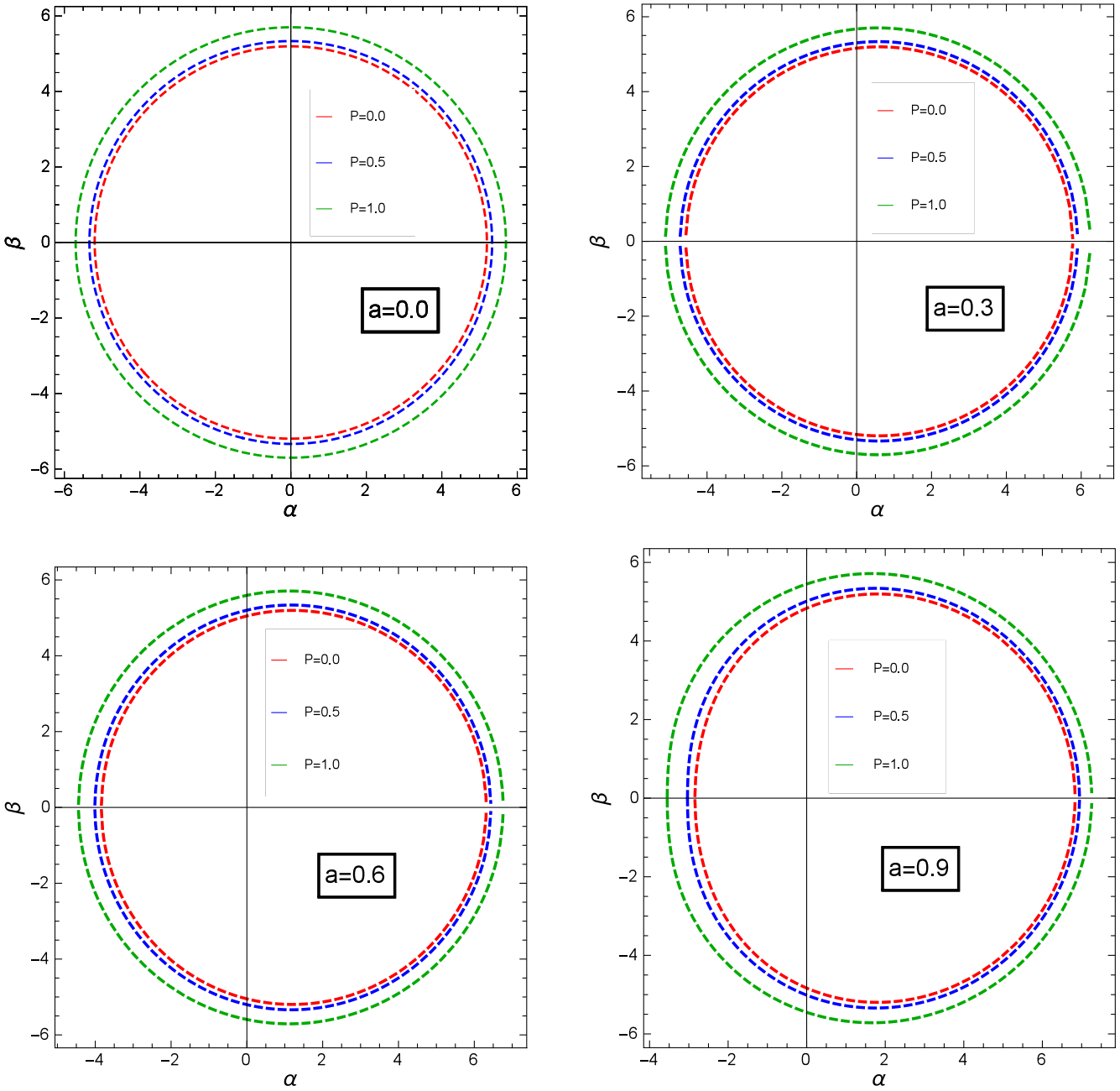

FIG. 4. Shadow casted by rotating black hole in generalized Proca theories given by the metric.(23) for different values of a and P as seen by observer in equatorial plane. The shadow region is corresponds to the inside of each dashed curve. The case $a = 0$ defines shadow for nonrotating black hole. An increase of a causes the deformation of the black hole shadow.

momentum J corresponds to counterclockwise winding of the light rays as seen from above. So when $a > 0$, the photons rotates in the same direction as the black hole (prograde/direct photons) while they rotate in the opposite direction for $a < 0$ case (retrograde photons). One can visualize the shape of black hole shadow by plotting β vs α. In Fig. 4, we have plotted the shadows casted by a black hole described by metric (23) for different values of a and P. Note that, for the nonrotating case ($a = 0$), the shadow of the black hole is just a dark circular disc. But when the black hole has a nonvanishing angular momentum ($a \neq 0$), the shape of the shadow gets slightly distorted. Moreover, it gets shifted towards right.

Following Ref. [65], we define the observables for black hole shadow as the radius R_s of a reference circle and the distortion parameter δ_s. We will consider a reference circle that passes through three points of the shadow: the top (α_t, β_t) and the bottom (α_b, β_b) and a point corresponds to the unstable retrograde circular orbit $(\alpha_r, 0)$. The distortion parameter δ_s is the ratio of the difference between the

endpoint of the circle $(\bar{\alpha}_p, 0)$ and the point corresponding to the prograde circular orbit $(\alpha_p, 0)$ [both of them at the opposite side of the point $(\alpha_r, 0)$] to radius of the reference circle [66]. Typically R_s gives the approximate size of the black hole shadow, while δ_s is a measure of its deformation with respect to the reference circle. For an equatorial observer, the observables take the form

$$R_s = \frac{(\alpha_t - \alpha_r)^2 + \beta_t^2}{2|\alpha_t - \alpha_r|} \tag{37}$$

$$\delta_s = \frac{\bar{\alpha}_p - \alpha_p}{R_s}. \tag{38}$$

By measuring this two observables, one can predict the black hole parameters very accurately. A simple way to extract the information about parameters a and P is to plot the contour curves of constant R_s and δ_s in the (a, P) plane [67]. The points in that plane where they intersect give the value of corresponding a and P. In Fig. 5, we show the contour plot of R_s and δ_s in the (a, P) plane. As stated earlier, if we can obtain values of R_s and δ_s very accurately from the observations, the point where the associated contours intersect, gives the corresponding values of a and P.

VII. GRAVITATIONAL LENSING BY A ROTATING BLACK HOLE IN STRONG FIELD LIMIT

In this section, we briefly review the main concepts and the observables related to strong lensing in a stationary, axisymmetric spacetime following the methods developed by Bozza [63]. Throughout our discussion, we have considered that both the source and observer are situated very far away from the black hole. For the sake of simplicity, we restrict our attention to the trajectories that are very close to the equatorial plane. Advantage of considering such a scenario is that the angular position of the images can still be described by those obtained in the equatorial plane but now one can understand the problem at some deeper level as one can calculate the magnification of the images from the two-dimensional lens equation.

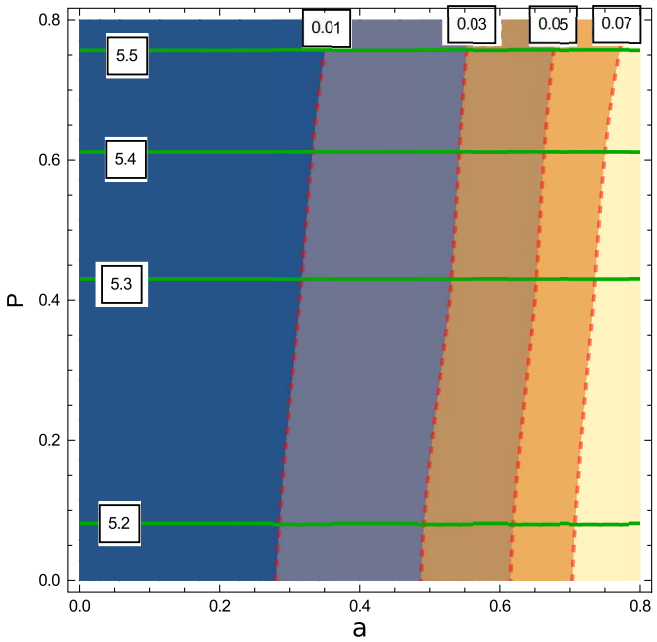

FIG. 5. The contour plot of constant R_s (green solid lines)and δ_s (red dashed lines) curves in the (a, P) plane have been presented. Intersection of the curves corresponding to constant R_s and δ_s obtained from observation gives value of a and P of the black hole.

We formulate the lensing problem as follows: we consider that the observer and the source are situated at a height h_R and h_S from the equatorial plane respectively. A photon with impact parameter u incoming from the source situated at r_S, approaches the black hole at a minimum distance r_0 and then deviates away from it. An observer at r_R receives the photon. Now we want to find the angular position and the magnification of the images. In order to do so, we first restrict our attention to the light rays on the equatorial plane by setting $\vartheta = \pi/2$ or equivalently by taking $\psi = \pi/2 - \vartheta = 0$ and $h = 0$. Substituting these conditions on Eq. (23), we get reduced metric of the form

$$ds^2 = -A(r)dt^2 + B(r)dr^2 + C(r)d\phi^2 - D(r)dtd\phi \tag{39}$$

In order to study the photon trajectory in a stationary spacetime, we assume that the equation [64]

$$(A_0C_0' - A_0'C_0)^2 = (A_0'D_0 - A_0D_0')(C_0'D_0 - C_0D_0') \tag{40}$$

admits at least one positive solution and largest positive root of the equation is defined as the radius of photon sphere, r_m. Here subscript '0' implies functions evaluated at closest approach distance r_0. Note that, when we put $D_0 = 0$, this equation coincides with the condition for photon sphere in static case given by Eq. (6). In the strong field limit, we consider only those photons whose closest approach distance r_0 is very near to r_m and hence the deflection angle α can be expanded around the photon sphere, r_m or equivalently minimum impact parameter u_m. When the closest approach distance r is greater than r_m, it just simply gets deflected (it may complete several loops around the black hole before reaching the observer). When it reaches a critical value $r_0 = r_m$ (or $u = u_m$), α diverges and the photon gets captured. Using the same method as in the case static case, we can express total deflection as follows [63],

$$\alpha_f(\theta) = -\bar{a}_{\rm rot} \log\left(\frac{\theta}{\theta_m} - 1\right) + \bar{b}_{\rm rot}, \tag{41}$$

where u_m is the impact parameter evaluated at r_m. The parameters $\bar{a}_{\rm rot}$, $\bar{b}_{\rm rot}$ are the strong field coefficient for rotating metric in the equatorial plane (for explicit

expression of $\bar{a}_{\rm rot}$, $\bar{b}_{\rm rot}$, see Eqs. (34)–(35) of Ref. [63]). θ denotes the angular position of the image. From Eq. (41), we can see that the deflection angle diverges at $\theta = \theta_m = u_m/r_R$. It represents the position of the innermost image. Once the deflection angle is known, we can obtain the angular position of different images using the lens equation (8). In the simplest situation, one can express the angular position of the n-th order image as [63]

$$\theta_n = \theta_n^0\left[1 - \frac{u_m e_n}{\bar{a}_{\rm rot}}\left(\frac{r_R + r_S}{r_R r_S}\right)\right] \tag{42}$$

where,

$$\theta_n^0 = \theta_m(1 + e_n), \qquad e_n = \exp\left[\frac{\bar{b}_{\rm rot} + \gamma - 2n\pi}{\bar{a}_{\rm rot}}\right].$$

Now we turn our attention to the trajectories that are very close to the equatorial plane; i.e., those trajectories have the very small value of declination angle $\psi = \pi/2 - \vartheta$. With the help of this condition and assuming the height of light ray trajectory from equatorial plane h is small compared to the projected impact parameter u, it is easy to show that the inclination angle $\psi_R \approx h/u$. The constants of motion given in Eqs. (35)–(36) can then be written as

$$J \approx u, \qquad Q \approx h^2 + \bar{u}^2\psi_R^2, \tag{43}$$

where $\bar{u} = \sqrt{u^2 - a^2}$. Moreover, we expect the declination angle ψ to remain small (of the order of ψ_R) during the motion. Small declination condition for the photon trajectory readily implies that $(h_R, h_S) \ll u \ll (r_R, r_S)$. If we neglect the higher order terms, then the polar lens equation can be written as [63]

$$\begin{aligned} h_S = {} & h_R\left[\frac{r_R}{\bar{u}}\sin\bar{\phi}_f - \cos\bar{\phi}_f\right] \\ & - \psi_R\left[(r_R + r_S)\cos\bar{\phi}_f - \frac{r_R r_S}{\bar{u}}\sin\bar{\phi}_f\right] \end{aligned} \tag{44}$$

where

$$\bar{\phi}_f(\theta) = -\hat{a}_{\rm rot}\ln\left(\frac{\theta}{\theta_m} - 1\right) + \hat{b}_{\rm rot} \tag{45}$$

Here, $\hat{a}_{\rm rot}$ and $\hat{b}_{\rm rot}$ denotes two numerical parameters (for more details see Eqs. (52)–(53) of Ref. [63]). Equation (44) along with Eq. (8) represents the two-dimensional lensing equation. Using these two equations, one can find we get the magnification of the nth image as

$$\mu_n = \frac{(r_R + r_S)^2}{(r_R r_S)}\left(\frac{\bar{\mu}(a)}{\mathcal{K}(\gamma)}\right) \tag{46}$$

where

$$\begin{aligned} \bar{\mu}(a) &= \frac{\bar{u}_m(a)u_m(a)e_\gamma}{\hat{a}_{\rm rot}(a)}, \qquad e_\gamma = \exp\left(\frac{\hat{b}_{\rm rot} + \gamma}{\hat{a}_{\rm rot}}\right), \\ \mathcal{K}(\gamma) &= r_R r_S \sin\bar{\phi}_{f,n} - \bar{u}_m(r_S + r_R)\cos\bar{\phi}_{f,n}. \end{aligned} \tag{47}$$

where $\bar{\phi}_{f,n}$ is the phase of the nth order image given by the Eq. (45) with θ_n is the solution of Eq. (42). Note that μ_n diverges when $\mathcal{K}(\gamma)$ vanishes. This condition gives the position of the caustic points which formally defined as the positions of source for which one gets infinite magnification of the images.

VIII. TIME DELAY BETWEEN DIFFERENT IMAGES IN STATIONARY SPACETIME

In this section we will extend our study of time delay effect in a rotating black hole spacetime. As stated earlier, formation of different image is a result of photons following different trajectories, time taken by different photons is not the same and hence there will be a time delay between them. Bozza [50] solved this problem using the same method used to find deflection angle and showed that the leading term in time delay between m-th and n-th order image can be expressed as [50]

$$\Delta T^s_{mn} = 2\pi(n - m)\frac{\tilde{a}_{\rm rot}(a)}{\bar{a}_{\rm rot}(a)} \tag{48}$$

When both the images are formed on the same side of the black hole. We can see that the time delay for direct photons ($a > 0$) and retrograde photons ($a < 0$) will be different.

When images are formed on the opposite side of the lens, then time delay between m-th and n-th order image can be expressed as [50]

$$\begin{aligned} \Delta T^o_{mn} = {} & \frac{\tilde{a}_{\rm rot}(a)}{\bar{a}_{\rm rot}(a)}(2\pi n + \gamma - \bar{b}_{\rm rot}(a)) + \tilde{b}_{\rm rot}(a) \\ & - \frac{\tilde{a}_{\rm rot}(-a)}{\bar{a}_{\rm rot}(-a)}(2\pi n - \gamma - \bar{b}_{\rm rot}(-a)) - \tilde{b}_{\rm rot}(-a) \end{aligned} \tag{49}$$

This extra contribution comes due to the fact that the coefficient $\bar{b}_{\rm rot}$ and $\tilde{b}_{\rm rot}$ is not same for direct and retrograde photons in the stationary case. The functional form of $\tilde{a}_{\rm rot}(a)$ and $\tilde{b}_{\rm rot}(a)$ is given in Eqs. (35)–(36) in Ref. [50].

IX. NUMERICAL ESTIMATION OF DIFFERENT OBSERVATIONAL PARAMETERS

In this section, we present the numerical estimation of different observational parameters related to strong lensing for stationary, axiasymmetric spacetime considering the SMBH at the center of our Galaxy as a lens. Here we have considered that nature of black hole spacetime is given by solutions of second order generalized Proca

theories presented in Eq. (23) and numerically estimated the values of different observables in the strong-field limit for two separate lensing configurations, namely, (a) when the source, lens, and the observer are highly aligned with the source and the observer is at infinity and (b) taking the star S2 as a source.

We have first considered a lensing system where the source, lens, and the observer are highly aligned and both the source and the observer are very far away from the lens. We numerically solved Eq. (40) to get the radius of the photon sphere r_m and angular radius of innermost image using the relation $\theta_m = u(r_m)/r_R$. We have further assumed that the outer most image θ_1 is resolved as a single image and all other images packed together at θ_m. Then the observables- angular separation between the inner- and outermost image s, the ratio of flux from the outermost image to those from all other image $\mathcal{R}$ and time delay between first and second relativistic image ΔT^s_{12} (formed on the same side of the lens) can be approximated by [45,50,68]

$$\begin{aligned} s &= \theta_1 - \theta_m \approx \theta_m \exp\left[\frac{\bar{b}_{\rm rot} - 2\pi}{\bar{a}_{\rm rot}}\right] \\ \mathcal{R} &= 2.5\log_{10}\left(\frac{\mu_1}{\sum_{n=2}^{\infty}\mu_n}\right) = \frac{5\pi}{\hat{a}_{\rm rot}\ln 10} \\ \Delta T^s_{12} &\approx 2\pi\frac{\tilde{a}_{\rm rot}(a)}{\bar{a}_{\rm rot}(a)} \end{aligned} \tag{50}$$

So by measuring θ_m, s and $\mathcal{R}$ we can correctly predict strong lensing co-efficient $\bar{a}_{\rm rot}$, $\bar{b}_{\rm rot}$ and the minimum impact parameter u_m and comparing them with the values predicted by a given theoretical model, we can identify the nature of the black hole. In Table IV, we have presented the numerical estimation of different observational parameters (θ_m, s, $\mathcal{R}$, ΔT^s_{12}). We also compare the results with those obtained from Kerr-Newmann (KN) black hole solution with charge q whose line element can be expressed as [69].

$$\begin{aligned} ds^2 = &-\left[1 - \frac{2Mr}{\rho^2} + \frac{q^2}{\rho^2}\right]dt^2 - \frac{4a\sin^2\vartheta}{\rho^2}\left[r - \frac{q^2}{2}\right]dtd\phi \\ &+ \frac{\rho^2}{\Delta_{\rm KN}}dr^2 + \rho^2 d\vartheta^2 \\ &+ \left[r^2 + a^2 + \frac{2ra^2\sin^2\vartheta}{\rho^2} - \frac{q^2a^2\sin^2\vartheta}{\rho^2}\right]\sin^2\vartheta d\phi^2 \end{aligned} \tag{51}$$

where

$$\Delta_{\rm KN} = r^2 - 2r + a^2 + q^2, \qquad \rho^2 = r^2 + a^2\cos^2\vartheta.$$

In Table IV, "hair" corresponds to Proca hair P in the case of rotating black holes in generalized Proca theories [Eq. (23)] and charged hair q in the case of Kerr-Newmann (KN) black holes [Eq. (51)]. We also have plotted the observables as a function of hair parameter for these two black hole spacetime in Fig. 6. From Table IV, we

TABLE IV. Numerical estimations of the observables related to strong lensing (θ_m, s, $\mathcal{R}$, ΔT^s_{12}) by a rotating black hole have been presented. A comparison between the values of the observables obtained from rotating black holes in generalized Proca theories (Proca BH) to those obtained from Kerr-Newmann black hole (KN BH) have also been presented. Here the parameter "hair" corresponds to Proca hair P in the case of rotating Proca BH and charged hair q in the case of Kerr-Newmann black holes. Note that, hair = 0 case corresponds to Kerr black hole. Here the SMBH at the center of our Galaxy is taken as the lens. We have assumed that the lensing system is highly aligned and both the source and observer are situated at infinity. The time delay between the first and second relativistic image ΔT^s_{12} have been calculated under the assumption that both of these images are formed on the same side of the lens.

		θ_m in μas		s in μas		$\mathcal{R}$		Time delay ΔT^s_{12}	
a	Hair	Proca BH	KN BH	Proca BH	KN BH	Proca BH	KN BH	Proca BH	KN BH
0.0	0.0	19.0033	19.0033	0.023 782 5	0.023 782 5	15.708	15.708	32.6484	32.6484
	0.2	19.0103	18.8756	0.024 150 3	0.024 371 1	15.6536	15.6367	32.6605	32.429
	0.4	19.0313	18.4796	0.025 286 7	0.026 399 6	15.4896	15.4039	32.6966	31.7488
	0.6	19.066	17.7691	0.027 294 3	0.031 020 6	15.2132	14.934	32.7563	30.5281
0.1	0 .0	18.2607	18.2607	0.029 515 1	0.029 515 1	15.708	15.708	31.3726	31.3726
	0.2	18.2666	18.1332	0.030 041 7	0.030 246 3	15.6413	15.6371	31.3829	31.1537
	0.4	18.2845	17.7382	0.031 675	0.032 756 8	15.4398	15.4058	31.4135	30.475
	0.6	18.314	17.0297	0.034 583 6	0.038 427 1	14.0986	14.9395	31.4642	29.2577
0.2	0.0	17.4932	17.4932	0.037 183 9	0.037 183 9	15.708	15.708	30.054	30.054
	0.2	17.4978	17.3667	0.037 956 1	0.038 079 1	15.6247	15.6388	30.0619	29.8367
	0.4	17.5115	16.9749	0.040 363 3	0.041 128 9	15.3721	15.4133	30.0855	29.1635
	0.6	17.5343	16.2738	0.044 688 4	0.047 884 4	15.9415	14.9618	30.1247	27.9591
0.3	0.0	16.6958	16.6958	0.047 692 4	0.047 692 4	15.708	15.708	28.684	28.684
	0.2	16.6986	16.5713	0.048 857	0.048 752	15.6018	15.6427	28.6889	28.4701
	0.4	16.707	16.1864	0.052 506V7	0.052 304 2	15.2765	15.4316	28.7033	27.8089
	0.6	16.7209	15.5015	0.059 122 6	0.059 865 3	14.7165	15.0155	28.7272	26.6322

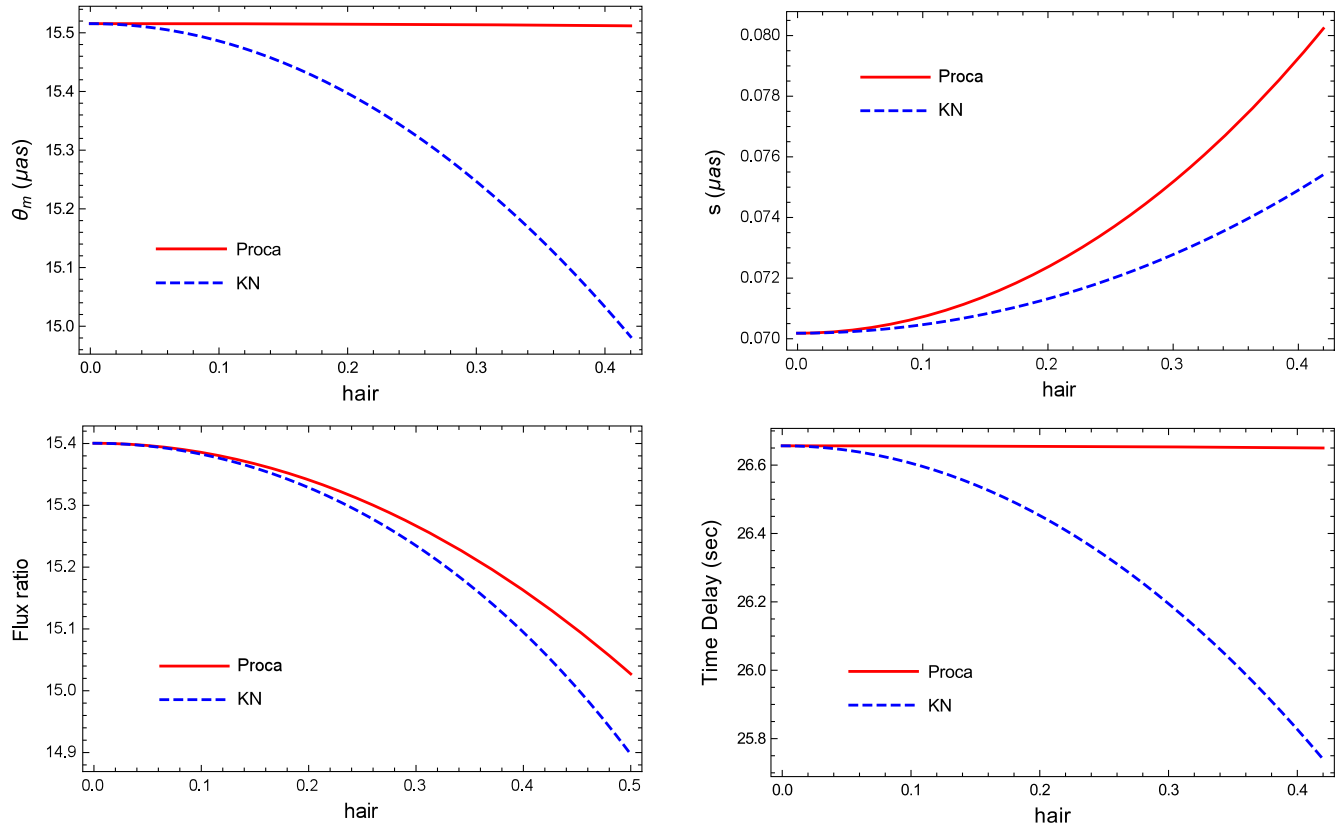

FIG. 6. Variation of different observables: (a) angular position of innermost image θ_m, (top-left corner) (b) the angular difference between the outermost and inner images s, (top-right corner) (c) Flux ratio of innermost image with respect to the others, $\mathcal{R}$ (bottom-left corner) and (d) Time delay between first and second relativistic image ΔT^s_{12} when both of these images are formed on the same side of the lens (bottom-right corner) as a function of the hair parameters have been presented. Here the parameter "hair" corresponds to Proca hair P in the case of rotating black hole in generalized Proca black holes and charge hair q in the case of Kerr-Newmann black holes. The solid red lines indicates the behavior of the observables as function Proca hair P for generalized Proca black holes whereas the blue dashed lines indices the variation of the observables as a function charge hair q for Kerr-Newmann black holes. Here we have assumed that the lensing system is highly aligned and both the source and observer are situated at infinity. We have taken that the value of the black hole spin is taken as $a = 0.44$, which is the current estimated value of spin of Sgr A$*$ [59].

can see that the angular position of the innermost image θ_m decreases with the increase of black hole spin a. But it increases with the increase of the hair parameter which is contrary to the KN case. Physically this implies that the size of the innermost Einstein ring is bigger for a slowly rotating black hole than those obtained from a rapidly rotating black hole. Moreover, that the size of the ring is bigger for the generalized Proca black holes spacetime than those obtained from Kerr-Newmann spacetime for the same value of the hair parameter. In Proca black hole spacetime, angular separation between the inner- and outermost image increases with the increase of a. This angular separation increases monotonically with the increase of the hair parameter similar to KN case. The relative flux $\mathcal{R}$ decreases with increase of both a and hair parameter similar to KN case. Now the time delay between first and second relativistic image (formed on the same side of the lens) ΔT^s_{12} increases with the increase of the hair parameter which is in contrary to the KN case. Note that size of the innermost Einstein ring θ_m (or, the time delay between first and second relativistic image ΔT^s_{12}) is maximum for the case a, $q = 0$ (Schwarzschild black hole) for the black holes predicted by general relativity. So any value of θ_m (or ΔT^s_{12}) greater than those predicted in Schwarzschild spacetime implies the existence of Proca hair. Thus by measuring the size of the innermost Einstein ring (or the time delay between first and second relativistic image), one can observationally verify the "no-hair theorem" [58]. Note that in Table IV we have considered a highly aligned lensing system, where both the source and observer are situated at infinity whereas, in Table II, we have taken S2 as a source. Now compare $a = 0$ case (corresponds to non-rotating black hole with source at infinity) for different values of the hair parameter presented in Table IV with the numerical values presented in Table II. Here one can see the value of the angular separation between the innermost and outermost image s is $\sim\mathcal{O}(10)$ times higher for later case than those presented in Table IV. Thus, the observable is in

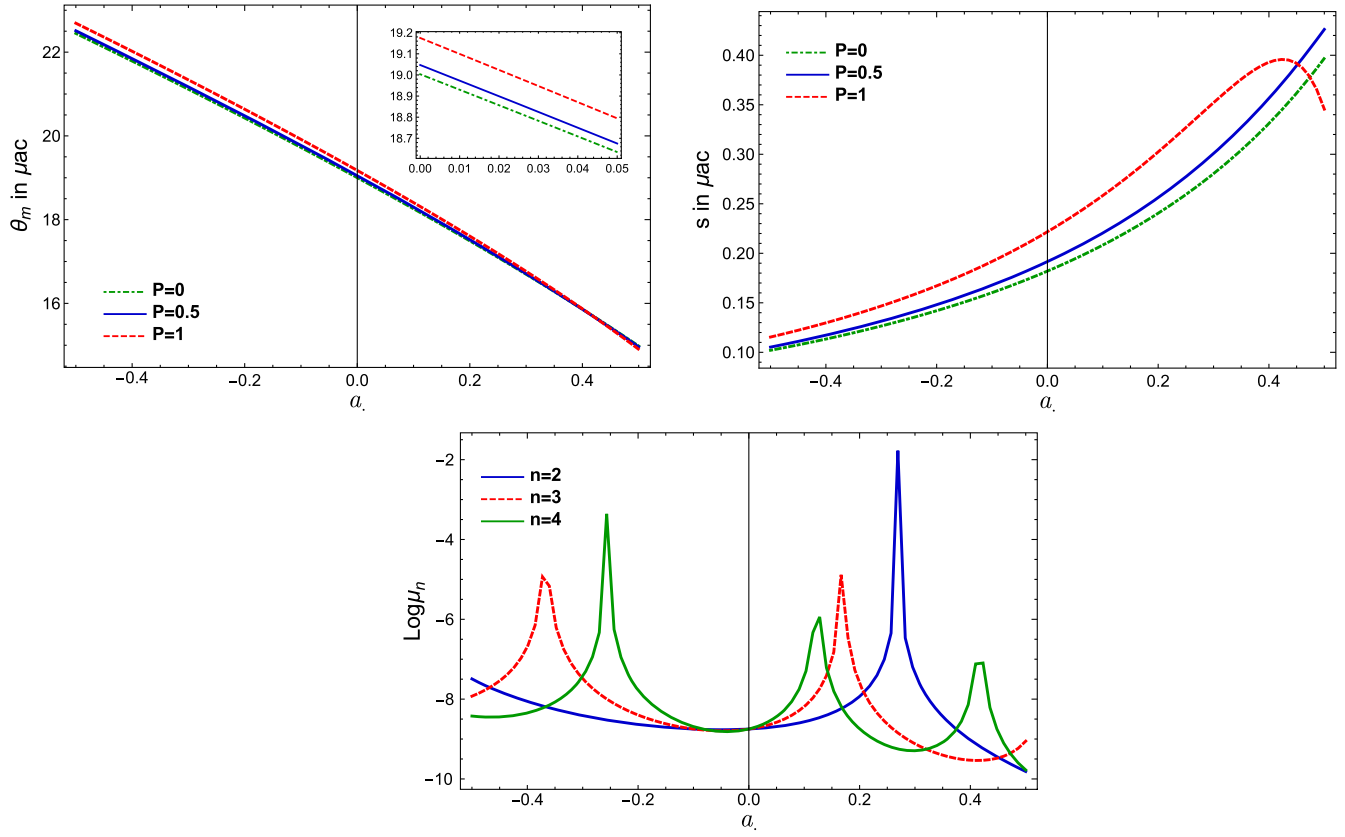

FIG. 7. Variation of different observables: (a) angular position of innermost image θ_m, (top-left corner) and (b) the angular difference between the outermost and innermost images s (top-right corner) for different values of Proca hair, (c) Magnification of second, third and fourth relativistic images, $\log \mu_n$ (bottom) as a function of black hole spin a have been presented. Here we have taken S2 as source. Note that the peaks in the magnification corresponds to caustic points. For drawing the caustics, we assume $P = 0.5$; but the overall behavior remains the same for other values of P.

more detectable range when one considers S2 as a source. However, still, the small value of angular separation ($\sim\mathcal{O}(10^{-1})\,\mu$ arc- sec) makes the detection of angular separation very difficult with present technologies.

Now we will turn our attention to the gravitational lensing by a rotating black hole in generalized Proca theories with S2 as a source. In this case a high alignment of the source with the optic axes does not happen due to inclination of the source orbit. So the simplified formula presented in Eq. (50) does not work in this case. Rather we have to relay on the more general formula of lensing given by Eqs. (42) and (46) to have correct estimation of angular position and the magnification of the images. Using those expression, we have plotted the observables θ_m (top-left corner), s (top-right corner) for different values of Proca hair P and the magnification of the images corresponding to different winding number n (bottom) as a function of a in Fig. 7. The peaks in the magnification corresponds to caustic points of the given lensing configuration where $\mathcal{K}(\gamma)$ vanishes [see Eq. (47)]. One can see that images corresponding to low winding number has fewer caustic points in the allowed range of a. As a result dimmer images meet caustic more often in the allowed range of a. For drawing the caustics, we assume $P = 0.5$; but the overall behavior remains the same for other values of P.

X. DISCUSSION AND CONCLUSION

In this paper, we discuss different astrophysical aspects for a black hole in second-order generalized Proca theories with derivative vector field interactions coupled to gravity. These black hole solutions are hairy and hence give us a perfect opportunity to observationally verify the "no-hair" theorem. We considered that the supermassive black hole in the center of the Galaxy is given by these generalized Proca theories and numerically estimated the values of different observables in the strong field limit for two separate lensing configurations, namely, (a) when the source, lens, and the observer are highly aligned and both the source and the observer are situated at infinity and (b) taking the star S2 as a source. For the latter case, we have shown that although the lensing system is not perfectly aligned, it gives observables in a more detectable range. In early 2018, S2 was at its periapse position, where one gets maximum magnification [51], and thus gave us a perfect opportunity to measure different lensing parameters.

We also compare our results with those obtained from the Reissner-Nordström (Kerr-Newmann for rotating case) black hole to see how the generalized Proca theory modifies the observables, taking the stationary black holes predicted by GR as a reference. Our study shows that the size of the innermost Einstein ring increases with the increase in Proca hair P for Proca black holes, whereas the Einstein ring will shrink with the increase of charge q for the Reissner-Nordström black hole (Kerr-Newmann for rotating case). The contribution of black hole spin can be well understood in the analysis of the black hole shadow. Adding angular momentum to a black hole will cause a slight distortion in the shape of the black hole shadow. Following Ref. [65], we have shown that by measuring this distortion with respect to a reference circle, one can accurately measure the black hole parameters (a, P). Thus, by analyzing black hole shadow, we can directly probe the black hole spacetime and hence the underlying gravity theory. With the prospects of the Even Horizon telescope as well as telescopes like SKA, one can resolve the black hole shadow with great accuracy and, hence, probing modified gravity through such observations is possible in the near future. The other two observable angular separations between inner- and outermost images and relative flux in between them exhibit the same behavior as in the case of the Reissner-Nordström black hole (Kerr-Newmann for rotating case) with the change of the hair parameter (which is Proca hair P for Proca black holes and charged hair q for Reissner-Nordström black hole). Angular separation between the images increases while the relative flux in between them decreases with the increase of the hair parameter. The time delay between first and second relativistic images, when both of them are formed on the same side of the lens, increases with the increase of the hair parameter which is in contrary to RN black hole (Kerr-Newmann for rotating case). The size of the innermost Einstein ring θ_m (or, the time delay between first and second relativistic image ΔT^s_{12}) is maximum for a, $q = 0$ case (Schwarzschild black hole) for the black holes predicted by general relativity. So any value of θ_m (or ΔT^s_{12}) greater than those predicted in Schwarzschild spacetime, implies the existence of Proca hair. Thus by measuring the size of the innermost Einstein ring (or the time delay between first and second relativistic image), one can observationally verify the "no-hair" theorem.

Unfortunately, the angular separation between the inner- and outermost relativistic image is extremely small ($\sim\mathcal{O}(10^{-1})$ μas while taking S2 as a source), which puts a great challenge for present technologies. However, modern near-infrared (NIR) instruments like PRIMA [70], GRAVITY [71], ASTRA [72] hope to achieve an astrometric accuracy of 10–100 μas in combination with milliarcsec angular-resolution imaging. With the help of these techniques, one can probe the Proca hair in near future.

ACKNOWLEDGMENTS

Research of M. R. is funded by the INSPIRE Fellowship (Reg. No. DST/INSPIRE/03/2015/003030) from Department of Science and Technology, Government of India.

[1] A. G. Riess *et al.*, Astron. J. **116**, 1009 (1998).
[2] S. Perlmutter *et al.*, Astrophys. J. **517**, 565 (1999).
[3] J. L. Tonry *et al.*, Astrophys. J. **594**, 1 (2003).
[4] R. A. Knop *et al.*, Astrophys. J. **598**, 102 (2003).
[5] A. G. Riess *et al.*, Astrophys. J. **607**, 665 (2004).
[6] E. J. Copeland, M. Sami, and S. Tsujikawa, Int. J. Mod. Phys. D **15**, 1753 (2006).
[7] T. Padmanabhan, Phys. Rep. **380**, 235 (2003).
[8] P. J. E. Peebles and B. Ratra, Rev. Mod. Phys. **75**, 559 (2003).
[9] V. Sahni and A. Starobinsky, Int. J. Mod. Phys. D **9**, 373 (2000).
[10] A. G. Riess *et al.*, Astrophys. J. **826**, 56 (2016).
[11] A. G. Riess *et al.*, Astrophys. J. **861**, 126 (2018).
[12] P. W. Higgs, Phys. Rev. Lett. **13**, 508 (1964); F. Englert, Phys. Rev. Lett. **13**, 321 (1964); T. W. B. Kibble, Phys. Rev. D **155**, 1554 (1967).
[13] J. Khoury and A. Weltman, Phys. Rev. Lett. **93**, 171104 (2004).
[14] A. I. Vainshtein, Phys. Lett. **39B**, 393 (1972).
[15] A. Nicolis, R. Rattazzi, and E. Trincherini, Phys. Rev. D **79**, 064036 (2009).
[16] C. Deffayet, G. Esposito-Farese, and A. Vikman, Phys. Rev. D **79**, 084003 (2009); C. Deffayet, S. Deser, and G. Esposito-Farese, Phys. Rev. D **80**, 064015 (2009); N. Chow and J. Khoury, Phys. Rev. D **80**, 024037 (2009).
[17] A. Ali, R. Gannouji, and M. Sami, Phys. Rev. D **82**, 103015 (2010); R. Gannouji and M. Sami, Phys. Rev. D **82**, 024011 (2010); A. De. Felice and S. Tsujikawa, Phys. Rev. Lett. **105**, 111301 (2010); S. A. Appleby and E. Linder, J. Cosmol. Astropart. Phys. 03 (2012) 043; E. Linder, J. Phys. Conf. Ser. **484**, 012006 (2014).
[18] G. R. Dvali, G. Gabaddze, and M. Porrati, Phys. Lett. B **485**, 208 (2000).
[19] M. A. Luty, M. Porrati, and R. Rattazzi, J. High Energy Phys. 09 (2003) 029; A. Nicolis and R. Rattazzi, J. High Energy Phys. 06 (2004) 059.
[20] R. P. Woodard, Lect. Notes Phys. **720**, 403 (2007).
[21] J. D. Barrow and M. Thorsrud, J. High Energy Phys. 02 (2013) 146; R. Kase and S. Tsujikawa, J. Cosmol. Astropart. Phys. 08 (2013) 054; C. Deffayet and D. A. Steer, Classical Quantum Gravity **30**, 214006 (2013); P. Martin-Moruno, N. J. Nunes, and F. S. N. Lobo, J. Cosmol. Astropart. Phys.

05 (2015) 033; A. de. Fellice, K. Koyama, and S. Tsujikawa, J. Cosmol. Astropart. Phys. 05 (2015) 058; S. Peirone, K. Koyama, L. Pogosian, M. Raveri, and A. Silvestri, Phys. Rev. D **97**, 043519 (2018).
[22] M. Fierz and W. Pauli, Proc. R. Soc. A **173**, 211 (1939); K. Hinterbichler, Rev. Mod. Phys. **84**, 671 (2012); M. V. Bebronne and P. G. Tinyakov, J. High Energy Phys. 04 (2009) 100; C. de Rham and L. Heisenberg, Phys. Rev. D **84**, 043503 (2011); L. Heisenberg and A. Refregier, J. Cosmol. Astropart. Phys. 09 (2016) 020.
[23] G. Tasinato, J. High Energy Phys. 04 (2014) 067.
[24] L. Heisenberg, J. Cosmol. Astropart. Phys. 05 (2014) 015.
[25] A. de. Felice, L. Heisenberg, R. Kase, S. Mukohyama, S. Tsujikawa, and Y-Li Zhang, J. Cosmol. Astropart. Phys. 06 (2016) 048; A. de. Felice, L. Heisenberg, R. Kase, S. Mukohyama, S. Tsujikawa, and Y-Li Zhang, Phys. Rev. D **94**, 044024 (2016); A. de. Felice, L. Heisenberg, and S. Tsujikawa, Phys. Rev. D **95**, 123540 (2017).
[26] L. Heisenberg, arXiv:1807.01725.
[27] B. P. Abott *et al.*, Phys. Rev. Lett. **116**, 061102 (2016).
[28] B. P. Abott *et al.*, Phys. Rev. Lett. **119**, 161101 (2017).
[29] P. Creminelli and F. Vernizzi, Phys. Rev. Lett. **119**, 251302 (2017); J. M. Ezquiaga and M. Zumalacárregui, Phys. Rev. Lett. **119**, 251304 (2017); J. Sakstein and B. Jain, Phys. Rev. Lett. **119**, 251303 (2017); L. Amendola, M. Kunz, I. D. Saltas, and I. Sawicki, Phys. Rev. Lett. **120**, 131101 (2018).
[30] J. Beltran Jimenez and L. Heisenberg, Phys. Lett. B **757**, 405 (2016); E. Allys, P. Peter, and Y. Rodriguez, J. Cosmol. Astropart. Phys. 02 (2016) 004.
[31] L. Heisenberg, R. Kase, M. Minamitsuji, and S. Tsujikawa, Phys. Rev. D **96**, 084049 (2017).
[32] P. Schneider, J. Ehlers, and E. E. Falco, *Gravitational Lenses* (Springer-Verlag, Berlin, 1992).
[33] S. Liebes, Phys. Rev. **B133**, 835 (1964).
[34] S. Refsdal and J. Surdej, Rep. Prog. Phys. **57**, 117 (1994).
[35] K. S. Virbhadra and G. F. R. Ellis, Phys. Rev. D **65**, 103004 (2002).
[36] E. F. Eiroa, G. E. Romero, and D. F. Torres, Phys. Rev. D **66**, 024010 (2002).
[37] V. Bozza, F. De Luca, and G. Scarpetta, Phys. Rev. D **74**, 063001 (2006); G. V. Kraniotis, Gen. Relativ. Gravit. **46**, 1818 (2014).
[38] R. Whisker, Phys. Rev. D **71**, 064004 (2005).
[39] S.-S. Zhao and Y. Xie, J. Cosmol. Astropart. Phys. 07 (2016) 007.
[40] S. Chakraborty and S. SenGupta, J. Cosmol. Astropart. Phys. 07 (2017) 045.
[41] P. V. P. Cunha, C. A. R. Herdeiro, E. Radu, and H. F. Runarsson, Phys. Rev. Lett. **115**, 211102 (2015).
[42] Ru-Sen Lu, A. E. Broderick, F. Baron, J. D. Monnier, V. L. Fish, S. S. Doeleman, and V. Pankratius, Astrophys. J. **788**, 120 (2014).
[43] R. Deane *et al.*, Proc. Sci. AASKA14 (**2015**) 151.
[44] L. Heisenberg, R. Kase, M. Minamitsuji, and S. Tsujikawa, J. Cosmol. Astropart. Phys. 08 (2017) 024.
[45] V. Bozza, Phys. Rev. D **66**, 103001 (2002).
[46] C. M. Claudel, K. S. Virbhadra, and G. F. R. Ellis, J. Math. Phys. (N.Y.) **42**, 818 (2001).
[47] A. Ishihara, Y. Suzuki, T. Ono, T. Kitamura, and H. Asada, Phys. Rev. D **94**, 084015 (2016).
[48] H. C. Ohanian, Am. J. Phys. **55**, 428 (1987).
[49] V. Bozza, Phys. Rev. D **78**, 103005 (2008).
[50] V. Bozza and L. Mancini, Gen. Relativ. Gravit. **36**, 435 (2004).
[51] V. Bozza and L. Mancini, Astrophys. J. **611**, 1045 (2004).
[52] A. Hees *et al.*, Phys. Rev. Lett. **118**, 211101 (2017).
[53] A. Boehle, A. M. Ghez, and R. Schödel *et al.*, Astrophys. J. **830**, 17 (2016); A. M. Ghez *et al.*, Astrophys. J. **689**, 1044 (2008).
[54] L. Meyer, A. M. Ghez, and R. Schödel, S. Yelda, A. Boehle, J. R. Lu, T. Do, M. R. Morris, E. E. Becklin, and K. Matthews, Science **338**, 84 (2012).
[55] A. Y. Bin-Nun, Phys. Rev. D **82**, 064009 (2010).
[56] H. Reissner, Ann. Phys. (Berlin) **355**, 106 (1916).
[57] S. Chandrasekhar, *The Mathematical Theory of Black Holes* (Oxford University Press, Oxford, 1983).
[58] C. W. Misner, K. S. Thorne, and J. A. Wheeler, *Gravitation* (W. H. Freeman, San Francisco, 1973); W. Israel, Phys. Rev. **164**, 1776 (1967); **164**, 1776 (1967); B. Carter, Phys. Rev. Lett. **26**, 331 (1971).
[59] Y. Kato, M. Miyoshi, R. Takahashi, H. Negoro, and R. Matsumoto, Mon. Not. R. Astron. Soc. **403**, L74 (2010).
[60] V. Bozza, F. De Luca, G. Scarpetta, and M. Sereno, Phys. Rev. D **72**, 083003 (2005).
[61] E. T. Newman and A. I. Janis, J. Math. Phys. (N.Y.) **6**, 915 (1965); S. P. Drake and P. Szekeres, Gen. Relativ. Gravit. **32**, 445 (2000).
[62] R. H. Boyer and R. W. Lindquist, J. Math. Phys. (N.Y.) **8**, 265 (1967).
[63] V. Bozza, Phys. Rev. D **67**, 103006 (2003).
[64] G. N. Gyulchev and S. S. Yazadjiev, Phys. Rev. D **75**, 023006 (2007).
[65] K. Hioki and K. i. Maeda, Phys. Rev. D **80**, 024042 (2009).
[66] L. Amarilla and E. F. Eiroa, Phys. Rev. D **85**, 064019 (2012); B. P. Singh, arXiv:1711.02898; A. Abdujabbarov, M. Amir, B. Ahmedov, and S. G. Ghosh, Phys. Rev. D **93**, 104004 (2016).
[67] L. Amarilla and E. F. Eiroa, Phys. Rev. D **87**, 044057 (2013).
[68] L. Ji, S. Chen, and J. Jing, J. High Energy Phys. 03 (2014) 089.
[69] E. T. Newman and A. I. Janis, J. Math. Phys. (N.Y.) **6**, 915 (1965); E. T. Newman, E. Couch, and K. Chinnapared, A. Exton, A. Prakash, and R. Torrence, J. Math. Phys. (N.Y.) **6**, 918 (1965).
[70] H. Bartko *et al.*, Proc. SPIE Int. Soc. Opt. Eng. **7013**, 4K (2008).
[71] F. Eisenhauer *et al.*, Proc. SPIE Int. Soc. Opt. Eng. **7013**, 2A (2008); V. Bozza and L. Mancini, Astrophys. J. **753**, 56 (2012).
[72] J. U. Pott *et al.*, New Astron. Rev. **53**, 363 (2009).